ACS APPLIED MATERIALS & INTERFACES

Letter

www.acsami.org

Improved Electrochemical Capacity of Precursor-Derived Si(B)CN-Carbon Nanotube Composite as Li-Ion Battery Anode

R. Bhandavat and G. Singh*

Department of Mechanical and Nuclear Engineering, Kansas State University, Manhattan, Kansas 66506, United States

Supporting Information

ABSTRACT: We study the electrochemical behavior of precursor-derived siliconboron carbonitride (Si(B)CN) ceramic and Si(B)CN coated-multiwalled carbon nanotube (CNT) composite as a lithium-ion battery anode. Reversible capacity of Si(B)CN was observed to be 138 mA h/g after 30 cycles, which is four times that of SiCN (~25 mA h/g) processed under similar conditions, while the Si(B)CN-CNT composite showed further enhancement demonstrating 412 mA h/g after 30 cycles. Improved performance of Si(B)CN is attributed to the presence of boron that is known to modify SiCN's nanodomain structure resulting in improved chemical stability and electronic conductivity. Post-cycling microscopy and chemical analysis of the anode revealed formation of a stable passivating layer, which resulted in stable cycling.

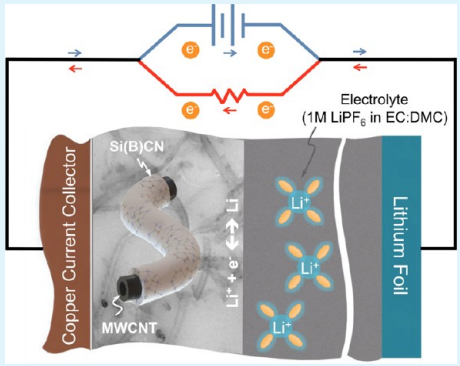

KEYWORDS: *precursor-derived ceramics, polysilazane, lithium-ion battery, electrochemical capacity, carbon nanotubes*

1. INTRODUCTION

Lithium-based secondary batteries such as the Li-ion battery (LIB) are currently being studied because of their ability to deliver high power and energy densities and longer cycle and shelf life.[1−3] Development of efficient and durable LIB mainly involves designing and testing of electrode and electrolyte materials with desired energy storage properties, rate capability, and synchronized performance. Ideally, a negative electrode material (anode) is expected to possess (a) high lithium ion storage ability, (b) ability to retain its physical and chemical structure with increasing number of cycles, (c) high ionic and electronic conductivity, and (d) maintain intimate contact with the current collector. Performance of conventionally used graphite anode in LIB mainly has a practical limitation of low capacity at higher operating current rates (e.g., reversible capacity of ~70 mA h/g when operating at 100 mA/g).[4] Several different materials and structures are currently being explored to address these requirements, of which the silicon-based nanostructures have received the most attention, primarily because of their high Li alloyability (theoretical capacity exceeding 4000 mA h/g) and low discharge potential that translates to a high power density.[5] But silicon's high electrochemical capacity comes at the cost of increased volume expansion (as much as 400%) that occurs upon lithiation. Subsequently, the delithation can cause several operational issues such as pulverization, delamination, and resulting capacity degradation especially for large-size battery anodes, making them incompetent for practical applications.[5] Although several solutions have been suggested, convincing results are yet to be seen.[6]

Silicon-based precursor-derived ceramics (PDCs) have been known for their unique amorphous structure that results in their high-temperature stability and mechanical strength, which in turn depends upon the starting precursor chemistry and processing conditions.[7,8] Recent studies on amorphous PDCs have highlighted their ability to store lithium in a reversible manner. These materials seem to outperform conventionally used graphite in terms of useful capacity and high rate performance.[4,9−17] In addition, composites made by blending PDCs with nanostructured materials like carbon nanotubes and graphene have also been explored for battery applications.[18−21]

The purpose of this work was to explore and measure the lithium cycling ability of Si(B)CN-CNT composite material. In our recent work we demonstrated synthesis of a boron-modified polymer that can be effectively utilized to synthesize Si(B)CN-CNT composite.[22] This composite offers improved oxidation resistance (stable in air up to 1000 °C) over SiCN-CNT composite.[22] Moreover, Si(B)CN ceramics have also been shown to have better electrical conductivity (as much as 4 orders of magnitude higher than SiCN).[23] Improved performance of boron-doped SiCN is generally attributed to the nanoscale changes happening in its amorphous structure such as rearrangement of -sp^2 carbon chains and formation of B(C)N domains.[23,24] In the present work, it is expected that the open nanodomain structure of amorphous Si(B)CN shell will lead to effective Li-ion diffusion and storage, whereas the nanotube core will improve the availability of electrons at

Received: August 6, 2012
Accepted: October 2, 2012
Published: October 2, 2012

   dx.doi.org/10.1021/am3015795 | ACS Appl. Mater. Interfaces 2012, 4, 5092−5097

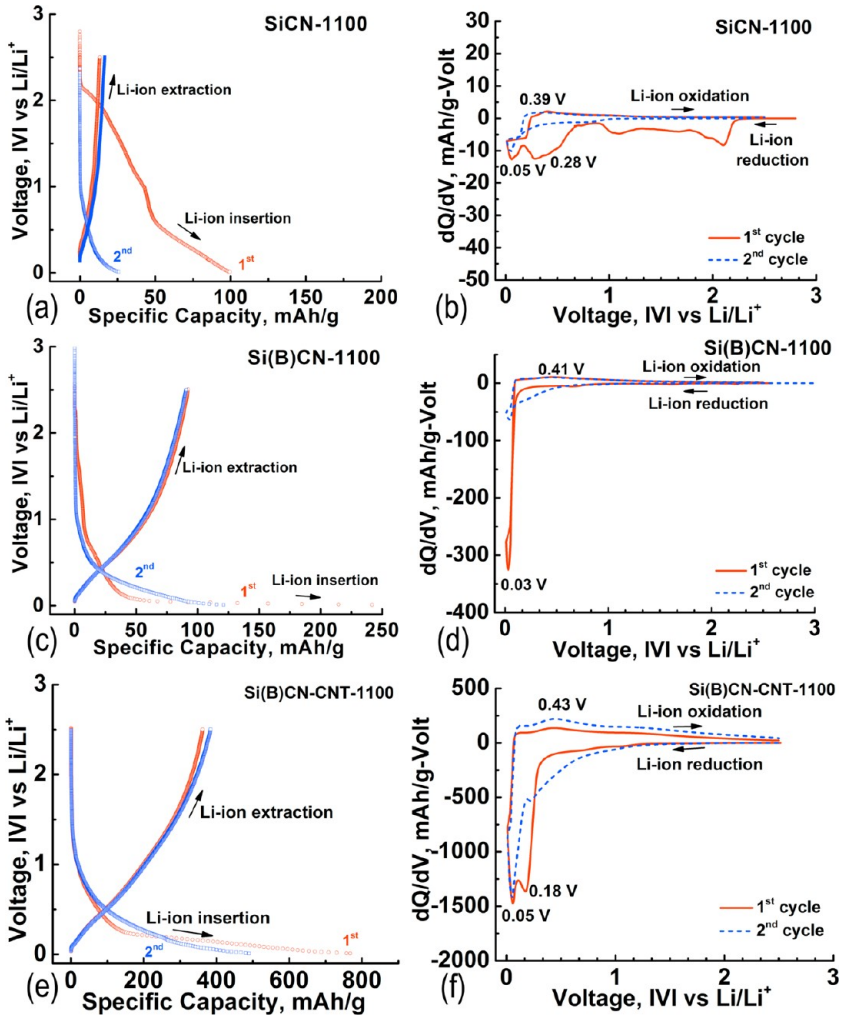

Figure 1. First and second electrochemical intercalation and deintercalation cycles and corresponding dQ/dV plots for (a, b) SiCN-1100, (c, d) Si(B)CN-1100, and (e, f) Si(B)CN-CNT-1100.

intercalation sites. Additionally, carbon nanotubes are expected to improve the mechanical toughness or long-term cycleability of the electrode.

To test this hypothesis of enhanced Li-ion cycling in PDCs by boron-doping and changing pyrolysis temperatures, we studied and compared lithium cycling behavior of SiCN (1100 °C), Si(B)CN (800, 1100, and 1500 °C) and Si(B)CN-CNT composites (800, 1100, and 1500 °C) anodes. Si(B)CN-CNT anodes processed at 1100 °C demonstrated a stable cycling performance with the highest reversible capacity and least first cycle loss.

2. EXPERIMENTAL PROCEDURE

Material Preparation. Polymer-derived Si(B)CN ceramic and Si(B)CN-CNT composite were prepared through controlled pyrolysis of a boron-modified polysilazane precursor reported in our earlier works.[22,25] In brief, commercially available polyureamethyl vinylsilazane (commercial name: Ceraset, Clariant) was modified using trimethyl borate reagent (Sigma Aldrich, 99.9%) to obtain polyborosilazane precursor. The precursor was then mixed with approximately 15 wt % CNTs (Bayer AG), which was followed by cross-linking at 400 °C for 2 h and pyrolysis at various temperatures (~800, ~1100, or ~1500 °C) for 4 h in flowing nitrogen resulting in formation of Si(B)CN-CNT shell/core composite.[22,25] While, the SiCN ceramic was prepared by cross-linking and pyrolysis of polyureamethylvinylsilazane at 400 and 1100 °C, respectively.[26−28]

Instrumentation. Structural characterization of the synthesized material and the battery anode was performed using 10 kV Carl Zeiss EVO Low-Vacuum SEM (Peabody, MA). Chemical composition of the specimen's surface was analyzed by X-ray photoelectron spectroscopy (XPS) using PHI Quantera SXM (Physical Electronics Inc. Chanhassen, MN) with monochromatic Al Kα X-radiation. Electrical conductivity measurements were carried out by use of a customized four-point probe setup and Keithley 2636A (Cleveland, OH) dual channel sourcemeter in the ohmic region. Electrochemical cycling of the assembled cells was carried out using multichannel Battery Test Equipment (Arbin-BT2000, Austin, TX) at atmospheric conditions.

Half-Cell Assembly and Testing. The working electrodes (anode) were prepared by mixing fine powdered active material (Si(B)CN or SiCN or Si(B)CN-CNT) with acetylene black and polyvinyl diflouride binder (1-methyl-2-pyrrolidinone) in the weight ratios of 8:1:1. Approximately 1−2 mg/cm^2 of the active material was then applied on the copper current collector foil by use of a doctor's blade and a film applicator. The coated foil was then dried at 100 °C for 12 h in an inert environment before using it as anode. The 2032 type cells were assembled, crimped and closed in a Argon filled glovebox. A 24 μm thick monolayer insulating membrane (Celgard) acted as the separator and approximately 1 mL electrolyte solution of 1 M $LiPF_6$ (Alfa Aesar) dissolved in (1:1 v/v) dimethyl carbonate: ethylene carbonate was used as the electrolyte. Pure lithium metal acted as both the counter and reference electrode. The cells were tested in the voltage range of 10 mV to 2.5 or 3 V at either 50 or 100

dx.doi.org/10.1021/am3015795 | ACS Appl. Mater. Interfaces 2012, 4, 5092−5097

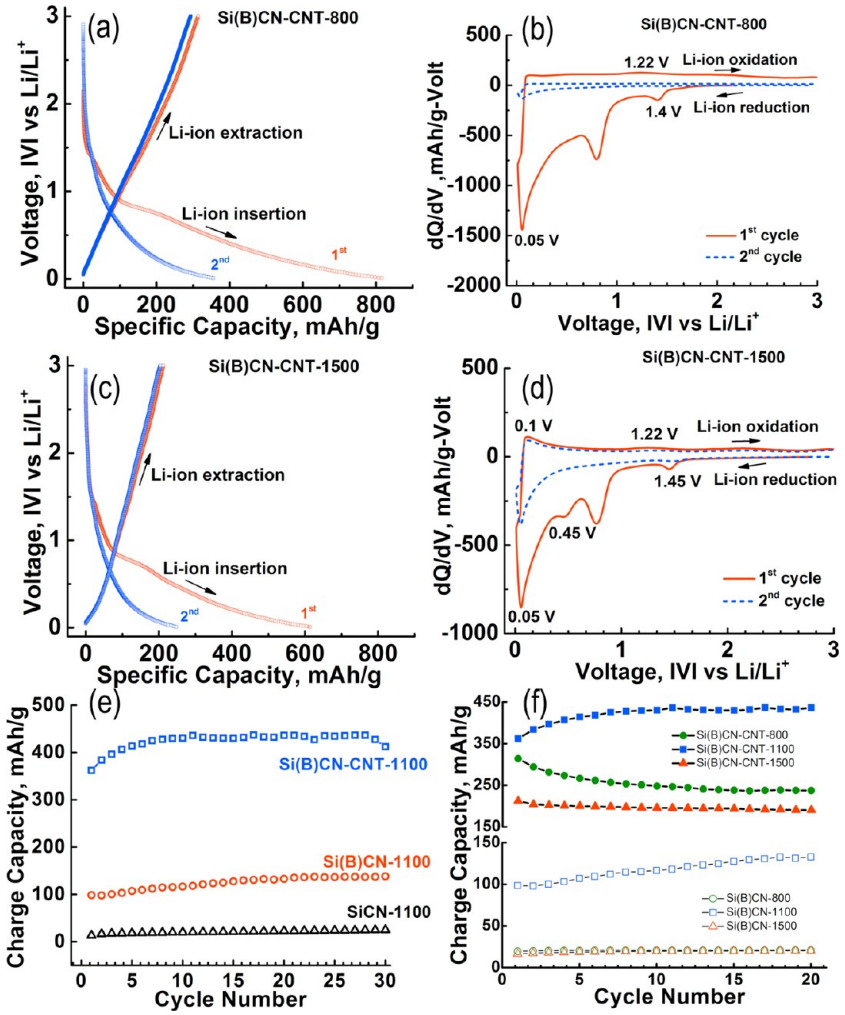

Figure 2. First two electrochemical voltage profiles and corresponding differentiated capacity with respect to the voltage for (a, b) Si(B)CN-CNT-800, (c, d) Si(B)CN-CNT-1500. Comparison of charge (reversible) capacity versus the cycle number for: (e) for SiCN-1100, Si(B)CN-1100 and Si(B)CN-CNT-1100 anodes, and (f) various Si(B)CN anodes showing the effect of pyrolysis temperature (20 cycles only).

mA/g during both discharge and charge half cycles. For the post-test characterization, the cells were disassembled inside the glovebox and the anodes were washed several times with dimethyl carbonate (DMC) to get rid of any excess electrolyte.

3. RESULTS AND DISCUSSION

Electrochemical Cycling Results. Figure 1a represents the first two-chronopotentiometric intercalation and deintercalation cycles of SiCN-1100 ceramic (complete polymer to ceramic conversion does not take place until 1000 °C and hence 1100 °C was the temperature of choice). The first cycle discharge and charge capacities were 99.4 and 13.2 mA h/g that dropped to 25.9 mA h/g and 16.5 mA h/g, respectively in the second cycle. This drop in electrochemical capacity is typical of SiCN prepared from the poylureasilazane (Ceraset) precursor,[4] thus resulting in a very high first cycle loss (ICL) of 86.6% with a voltage hysteresis of 0.77 V. However, the Si(B)CN-1100 ceramic specimen synthesized and cycled under similar conditions (Figure 1c) showed higher first discharge (241.9 mA h/g) and charge (98.5 mA h/g) capacities with a first cycle loss of 59.3%. The Si(B)CN-CNT-1100 composite anode showed further enhancement in the electrochemical capacity as compared with Si(B)CN and SiCN processed under similar conditions (Figure 1e). A high reversible capacity (312.1 mA h/g) and relatively low first cycle loss (45.5%) were observed.

The results were also the best when compared with other Si(B)CN-CNT specimen, i.e., those processed at 800 and 1500 °C (Figure 2). The dependence of electrochemical capacity on specimen pyrolysis temperature is similar to and is in agreement with recent electrochemical studies on SiCN and SiOC ceramics.[4,14,16,29] The Si(B)CN-CNT-1100 anode also showed higher reversible capacity and better capacity retention when compared to some other PDC-based anodes reported in the literature such as C-rich SiCN (reversible capacity of ~263 mA h/g)[13] and SiCN/graphite (reversible capacity of 374 mA h/g).[20]

The initial cycle capacity values and other critical evaluation parameters like the first cycle loss and capacity retention for SiCN and Si(B)CN anodes are summarized in Table 1.

Differentiated capacity with respect to voltage (dQ/dV) plots for SiCN, Si(B)CN, and various Si(B)CN-CNT specimen are plotted in Figure 1b, d, and e and Figure 2b, d. A dQ/dV peak position signifies the amount of Li-ions diffusing in or out of the host material at a given voltage. For SiCN anode first cycle (Figure 1b), major reduction peaks at ~50 mV and ~0.28 V suggests Li-ion intercalation in SiCN pores and free or graphitic carbon entities in SiCN ceramics, respectively.[14,15] The weak

dx.doi.org/10.1021/am3015795 | ACS Appl. Mater. Interfaces 2012, 4, 5092−5097

Table 1. Summary of Electrochemical Cycling Data for Various Specimens. The Error in the Measurements is ±0.1%

specimen	1st discharge capacity (mA h/g)	1st charge capacity (mA h/g)	first cycle loss (%)	charge capacity at (n^{th} cycle)
SiCN-1100	99.4	13.2	86.6	24.8 (30)
Si(B)CN-800	52.8	19.5	63.1	20.7 (20)
Si(B)CN-1100	241.9	98.5	59.3	138.2 (30)
Si(B)CN-1500	48.1	16.5	65.7	20.2 (20)
Si(B)CN-CNT-800	815.4	314	61.5	237.3 (20)
Si(B)CN-CNT-1100	768.1	361.9	52.9	412.1 (30)
Si(B)CN-CNT-1500	613.5	212.4	65.4	190.7 (20)

peak at 50 mV reappears in the second cycle. A small oxidation peak at ∼0.39 V was also observed for both first and second cycles, whereas for Si(B)CN anode (Figure 1d), one strong reduction peak at ∼30 mV indicate single reduction energy state for both first and second intercalation cycles.

For all Si(B)CN-CNT specimens, the dQ/dV plot showed multiple Li-ion reduction peaks majorly at ∼50 mV, ∼0.45, and ∼0.8 V (Figures 1f and 2b, d). As observed in Figure 1d, reduction peak at ∼50 mV is attributed to Si(B)CN ceramic, whereas the peaks at 0.45 and 0.8 V suggests existence of multiple intercalation phases .[5,30] The additional peak observed for 800 and 1500 °C specimens at ∼1.45 V, could have originated because of the presence of hydrogen (800 °C) or crystalline nature (1500 °C) of the specimen.[4,15] Broad peaks suggest availability of multiple Li-ion intercalation phases in the ceramic host material.

The variation in electrochemical cycling with changing pyrolysis temperature (Figures 1e and 2a, c), implies its dependence on molecular arrangement of ceramic constituents. This is not surprising since chemical co-ordinations in PDCs have been known to depend on the pyrolysis temperature of the precursor. Pyrolysis at 800 °C has been known to result in a mix of organic and inorganic compounds along with the presence of excess hydrocarbons,[31] whereas pyrolysis in the temperature range of 1000−1400 °C results in the formation of quaternary silicon possessing mixed bonds tetrahedral (Si−C−N), sp^2-bonded carbon chains and turbostratic B(C)N domains.[23] The electrochemical performance can be thus be correlated with the carbon structure in the specimens. The presence of soft, disordered, or hydrogenated carbon could be responsible for lithium ion irreversibility for the specimen synthesized at 800 °C,[13,20] whereas for the specimen pyrolyzed at 1500 °C or higher temperatures, Si(B)CN starts to undergo phase separation forming crystalline domains of Si_3N_4, SiC, and BN that are inactive to lithium cycling (see XRD data in Figure S1 and HR-TEM data in Figure S2 of the Supporting Information). Additionally, the abundance of dangling Si bonds for 800 °C specimen as compared to the 1100 °C specimens results in higher first cycle discharge capacity and higher irreversibility.[16] Hence, the 800 °C specimen (mostly disordered carbon) or crystalline nature of 1500 °C specimen (with turbostratic carbon or B(C)N) results in lower reversible electrochemical capacity and performance than the 1100 °C specimen.

The comparison of Li-ion reversible capacities of SiCN-1100, Si(B)CN-1100 and Si(B)CN-CNT-1100 specimens tested for 30 cycles are shown in Figure 2e. Although the electrochemical capacities for SiCN-1100 and Si(B)CN-1100 specimens were low, they retained the initial reversible capacity even after 30 cycles with more than 90% cyclic efficiency. We also studied the electrochemical performance of MWCNT anode (prepared and cycled under similar conditions) for comparison purposes (please see Figure S3 in the Supporting Information). The MWCNT anode showed a low first cycle charge capacity of ∼147.2 mA h/g (with a first cycle loss of 74.82%), which decreased further to ∼115.24 mA h/g after 30 cycles.

The effect of pyrolysis temperature on the long-term cycling performance of Si(B)CN-CNT specimens is presented in Figure 2f (Please note that data for the 1100 °C specimens is repeated here for ease of comparison). It is apparent that inclusion of boron in SiCN ceramic results in both higher reversible capacity and better capacity retention. Further, the ab initio approach of blending CNTs with ceramic precursor to form a core shell structure (see Figure S2 in the Supporting Information) results in better performance on all critical performance parameters.

Galvanostatic intermittent titration technique (GITT) was performed to get an approximation of the solid state Li-ion diffusion coefficient (D_{Li}) for Si(B)CN-CNT-1100 anode (best performing anode). Please see section IV of the Supporting Information for experimental details. The calculated D_{Li} varied between (1.5×10^{-8} and 4.9×10^{-7}) m^2/s during intercalation and (2.3×10^{-9} and 5.7×10^{-8}) m^2/s during extraction (as can be seen in Figure S4 in the Supporting Information). These values are about 3 orders of magnitude higher than those reported for polymer-derived SiOC anode (varied between 10^{-14} and 10^{-11}) m^2/s,[32] whereas for silicon anodes, D_{Li} has a range of (1×10^{-17} and 2×10^{-14}) m^2/s.[33,34]

Electrical conductivity measured using four point setup (see Figure S5 in the Supporting Information), for the Si(B)CN pellets specimens synthesized at 800, 1100, and 1500 °C were 1×10^{-4} S/cm, 8.7×10^{-4} S/cm, and 1.3×10^{-2} S/cm, respectively. Increased conductivity was observed for Si(B)CN-CNT powdered specimens synthesized at 800, 1100, and 1500 °C, which were 7.6×10^{-3} S/cm, 2.3×10^{-2} S/cm, and 1.2×10^{-1} S/cm, respectively. Whereas the measuring instrument was found insensitive to SiCN-1100 pellet specimen, but reasonable room temperature conductivity of $\sim 1 \times 10^{-7}$ S/cm have been reported elsewhere that can be used for comparison purposes.[23] For the dispersed (and dried) MWCNT pellet specimen, the electrical conductivity was approximately 0.25 S/cm. Thus, the increased electrical conductivity seems to influence the enhanced performance of Si(B)CN-CNT than Si(B)CN and SiCN, as easier flow of electrons in the electrode microstructure is desirable for easier and efficient Li-ion anode cycling.

Postelectrochemical Cycling Characterization. The cycled cells were dissembled and the anodes were recovered for post electrochemical cycling analysis. SEM imaging was performed for SiCN, Si(B)CN and Si(B)CN-CNT anodes and their surface morphology was compared with their respective precycled anodes (Figure 3). Precycled SiCN and Si(B)CN anodes exhibited a particle (size <500 nm) like morphology. Interconnected particles with sponge like (fluffy) carbon black

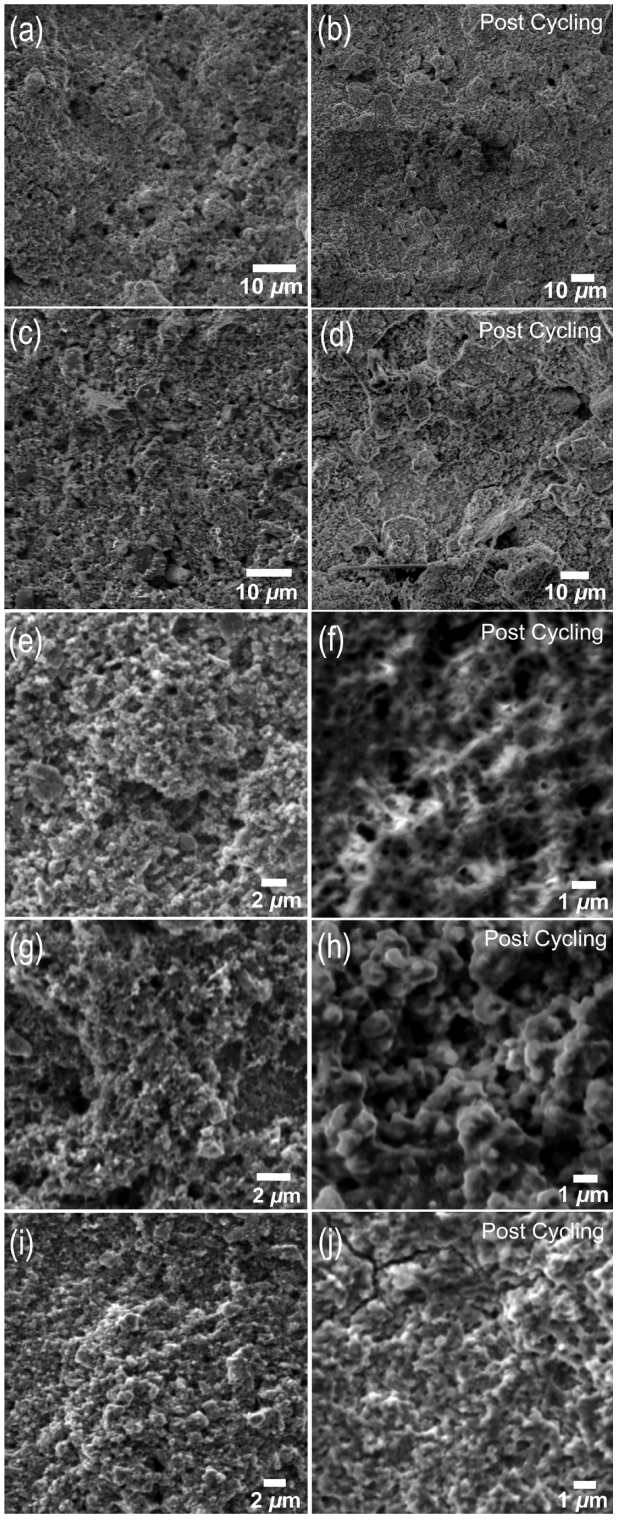

Figure 3. Comparison of SEM images of "as-prepared" anodes with the cycled anodes (disassembled in delithiated state) for (a, b) SiCN-1100 (after 30 cycles), (c, d) Si(B)CN-1100 (after 30 cycles), (e, f) Si(B)CN-CNT-800 (after 20 cycles), (g, h) Si(B)CN-CNT-1100 (after 30 cycles), and (i, j) Si(B)CN-CNT-1500 (after 30 cycles).

were also observed. The Si(B)CN-CNT anodes were porous with a matrix like appearance.

Remarkably, all cycled anodes were largely intact with no obvious signs of delamination or pulverization. Unlike bulk silicon or thin films, where lithium cycling results in surface cracks due to volume expansion, absence of surface cracks in these anodes suggested very stable cyling with minimal structural changes.[5] The cycled Si(B)CN-CNT-800, exhibited amorphous (soft) porous coating, whereas the cycled Si(B)CN-CNT-1500 specimen showed formation of a few surface cracks. Si(B)CN-CNT-1100 specimen showed the firmly integrated structure corroborating the best electrochemical performance results shown earlier. The presence of SEI (solid electrolyte interphase) layer looked more prominent on the Si(B)CN-CNT electrode surface than on either SiCN or Si(B)CN anodes, as could be seen in the post-cycling SEM images.

XPS survey scan performed on dissembled SiCN-1100, Si(B)CN-1100, and Si(B)CN-CNT-800 anodes, revealed presence of Si, C, Li, O, F and P elements (see Figure S6 in the Supporting Information). As shown in Figure S6 in the Supporting Information, for the SiCN anode, the Si2p elemental peak observed at ∼102.5 eV can be deconvoluted into peaks at 103.2 and 102.1 eV due to Si−O and Si−N−O type bonds, respectively.[35] The C1s peak at ∼285 eV can be assigned to peaks at 285.7, 285, and 283.8 eV due to sp^2 carbon, Li−C−H−N, and Si−C, respectively. For the Si(B)CN anode, the sharp peak at ∼102.5 eV can be fitted by two peaks at 103 eV (Si−O) and 101.9 eV (Si−N). While the lower energy peak in C1s scan at ∼284.9 eV is assigned to sp^2-bonded carbon and the higher energy peak at 293.7 eV is most likely due to the C−F−O bonds from the SEI layer.[36] The Si2p elemental scan for the Si(B)CN-CNT anode showed a less intense peak at ∼102.5 eV which can originate from Si−O−N type bonds. The lower energy peak in the C1s scan at ∼284.8 eV is assigned to sp^2 bonded carbon whereas the higher energy peak at ∼289.8 eV is due to Li_2CO_3 most likely from SEI layer that gets formed on the anode's surface. Based on the postcycling imaging and XPS analysis, it is safe to assume that formation of a stable SEI layer on the anode surface was another reason for the stable Li-cycling observed in the Si(B)CN-CNT-1100 specimen.

4. CONCLUSION

Si(B)CN ceramic derived from controlled thermal decomposition (pyrolysis) of boron-modified polyureasilazane showed improved Li-ion storage ability and sustained capacity when utilized as battery anode. Further, nanocomposites prepared by inclusion of CNTs in liquid phase polymeric precursor resulted in core−shell Si(B)CN-CNT morphology, which further enhanced the electrochemical capacity by four folds. This improved behavior is attributed to the structurally porous and thermodynamically stable Si(B)CN shell and electrically conducting CNT core.

■ ASSOCIATED CONTENT

Supporting Information

XRD and XPS data, and details on conductivity measurement procedure. This material is available free of charge via the Internet at http://pubs.acs.org.

■ AUTHOR INFORMATION

Corresponding Author

*E-mail: gurpreet@ksu.edu. Tel.: +1-785-532-7085. Fax: +1-785-532-7057.

Notes

The authors declare no competing financial interest.

■ ACKNOWLEDGMENTS

This research is based on work supported by the National Science Foundation under Grant EPS-0903806 and the State of Kansas through Kansas Technology Enterprise Corporation. The authors would like to thank Professor Rishi Raj (University of Colorado at Boulder) and Dr. Dongjoon Ahn (GM Research, Warren, MI) for introducing us to lithium-ion battery research and Dr. Jerry Hunter (Virginia Tech) for XPS.

■ REFERENCES

(1) Kamat, P. V. *J. Phys. Chem. Lett.* **2010**, *1*, 2220−2221.
(2) Kamat, P. V. *J. Phys. Chem. Lett.* **2011**, *2*, 242−251.
(3) Manthiram, A. *J. Phys. Chem. Lett.* **2011**, *2*, 176−184.
(4) Ahn, D.; Raj, R. *J. Power Sources* **2011**, *196*, 2179−2186.
(5) Ruffo, R.; Hong, S. S.; Chan, C. K.; Huggins, R. A.; Cui, Y. *J. Phys. Chem. C* **2009**, *113*, 11390−11398.
(6) Luo, J.; Zhao, X.; Wu, J.; Jang, H.; Kung, H.; Huang, J. *J. Phys. Chem. Lett.* **2012**, *3*, 1824−1829.
(7) Bill, J.; Aldinger, F. *Adv. Mater.* **1995**, *7*, 775−787.
(8) Weinmann, M.; Schuhmacher, J.; Kummer, H.; Prinz, S.; Peng, J. Q.; Seifert, H. J.; Christ, M.; Muller, K.; Bill, J.; Aldinger, F. *Chem. Mater.* **2000**, *12*, 623.
(9) Ahn, D.; Raj, R. *J. Power Sources* **2010**, *195*, 3900−3906.
(10) Feng, Y. *Electrochim. Acta* **2010**, *55*, 5860−5866.
(11) Fukui, H.; Nakata, N.; Dokko, K.; Takemura, B.; Ohsuka, H.; Hino, T.; Kanamura, K. *ACS Appl. Mater. Interfaces* **2011**, *3*, 2318−2322.
(12) Fukui, H.; Ohsuka, H.; Hino, T.; Kanamura, K. *J. Electrochem. Soc.* **2011**, *158*, A550−A555.
(13) Graczyk-Zajac, M.; Mera, G.; Kaspar, J.; Riedel, R. *J. Eur. Ceram. Soc.* **2010**, *30*, 3235−3243.
(14) Kaspar, J.; Mera, G.; Nowak, A. P.; Graczyk-Zajac, M.; Riedel, R. *Electrochim. Acta* **2010**, *56*, 174−182.
(15) Liebau-Kunzmann, V.; Fasel, C.; Kolb, R.; Riedel, R. *J. Eur. Ceram. Soc.* **2006**, *26*, 3897−3901.
(16) Su, D.; Li, Y.; Feng, Y.; Jin, J. *J. Am. Ceram. Soc.* **2009**, *92*, 2962−2968.
(17) Tamai, H.; Sugahara, H.; Yasuda, H. *J. Mater. Sci. Lett.* **2000**, *19*, 53−56.
(18) Feng, Y.; Du, G.; Zhao, X.; Yang, E. *J. Appl. Electrochem.* **2011**, *41*, 999−1002.
(19) Feng, Y.; Feng, N.; Du, G. *Int. J. Electrochem. Sc.* **2012**, *7*, 3135−3140.
(20) Graczyk-Zajac, M.; Fasel, C.; Riedel, R. *J. Power Sources* **2011**, *196*, 6412−6418.
(21) Kolb, R.; Fasel, C.; Liebau-Kunzmann, V.; Riedel, R. *J. Eur. Ceram. Soc.* **2006**, *26*, 3903−3908.
(22) Bhandavat, R.; Singh, G. *J. Am. Ceram. Soc.* **2012**, *95*, 1536−1543.
(23) Hermann, A. M.; Wang, Y. T.; Ramakrishnan, P. A.; Balzar, D.; An, L. N.; Haluschka, C.; Riedel, R. *J. Am. Ceram. Soc.* **2001**, *84*, 2260−2264.
(24) Sarkar, S.; Gan, Z.; An, L.; Zhai, L. *J. Phys. Chem. C* **2011**, *115* (50), 24993−25000.
(25) Bhandavat, R.; Kuhn, W.; Mansfield, E.; Lehman, J.; Singh, G. *ACS Appl. Mater. Interfaces* **2012**, *4*, 11−16.
(26) Lehman, J. H.; Hurst, K. E.; Singh, G.; Mansfield, E.; Perkins, J. D.; Cromer, C. L. *J. Mater. Sci.* **2010**, *45*, 4251−4254.
(27) Shah, S. R.; Raj, R. *J. Eur. Ceram. Soc.* **2005**, *25*, 243−249.
(28) Singh, G.; Priya, S.; Hossu, M. R.; Shah, S. R.; Grover, S.; Koymen, A. R.; Mahajan, R. L. *Mater. Lett.* **2009**, *63*, 2435−2438.
(29) Dibandjo, P.; Graczyk-Zajac, M.; Riedel, R.; Pradeep, V. S.; Soraru, G. D. *J. Eur. Ceram. Soc.* **2012**, *32*, 2495−2503.
(30) Landi, B. J.; Dileo, R. A.; Schauerman, C. M.; Cress, C. D.; Ganter, M. J.; Raffaelle, R. P. *J. Nanosci. Nanotechnol.* **2009**, *9*, 3406−3410.
(31) Greil, P. *Adv. Eng. Mater.* **2000**, *2*, 339−348.
(32) Ahn, D. Electrochemical Insertion of Lithium into Polymer Derived Silicon Oxycarbide and Oxycarbonitride Ceramics. Ph.D. Thesis, University of Colorado, Boulder, CO, 2010
(33) Ruffo, R.; Hong, S. S.; Chan, C. K.; Huggins, R. A.; Cui, Y. *J. Phys. Chem. C* **2009**, *113*, 11390−11398.
(34) Kulova, T. L.; Skundin, A. M.; Pleskov, Y. V.; Terukov, E. I.; Kon'kov, O. I. *J. Electroanal. Chem.* **2007**, *600*, 217−225.
(35) Wagner, C. D.; Naumkin, A. V.; Vass, A. V.; Allison, J. W.; Powell, C. J.; Rumble, R. J. NIST X-ray Photoelectron Spectroscopy Database [Online], August 27, 2007. http://srdata.nist.gov/xps/ (accessed June 06, 2012).
(36) Tasaki, K.; Harris, S. J. *J. Phys. Chem. C* **2010**, *114*, 8076−8083.